

Original Article

Mitochondrial dysfunction reduces the activity of KIR2.1 K⁺ channel in myoblasts via impaired oxidative phosphorylation

JooHan Woo^{1,#}, Hyun Jong Kim^{2,3,#}, Yu Ran Nam^{2,3}, Yung Kyu Kim², Eun Ju Lee⁴, Inho Choi⁴, Sung Joon Kim¹, Wan Lee^{3,5,*}, and Joo Hyun Nam^{2,3,*}

¹Department of Biomedical Sciences, Seoul National University College of Medicine, Seoul 03080, ²Department of Physiology, Dongguk University College of Medicine, Gyeongju 38066, ³Channelopathy Research Center (CRC), Dongguk University College of Medicine, Goyang 10326, ⁴Department of Medical Biotechnology, Yeungnam University, Gyeongsan 38541, ⁵Department of Biochemistry, Dongguk University College of Medicine, Gyeongju 38066, Korea

ARTICLE INFO

Received July 16, 2018
Revised August 28, 2018
Accepted August 29, 2018

*Correspondence

Wan Lee
E-mail: wanlee@dongguk.ac.kr
Joo Hyun Nam
E-mail: jhnam@dongguk.ac.kr

Key Words

Inward-rectifying K⁺ channel
MtDNA-depleted myoblasts
Myoblast
Myogenesis
Oxidative phosphorylation

#These authors contributed equally to this work.

ABSTRACT Myoblast fusion depends on mitochondrial integrity and intracellular Ca²⁺ signaling regulated by various ion channels. In this study, we investigated the ionic currents associated with [Ca²⁺]_i regulation in normal and mitochondrial DNA-depleted (ρ0) L6 myoblasts. The ρ0 myoblasts showed impaired myotube formation. The inwardly rectifying K⁺ current (I_{Kir}) was largely decreased with reduced expression of KIR2.1, whereas the voltage-operated Ca²⁺ channel and Ca²⁺-activated K⁺ channel currents were intact. Sustained inhibition of mitochondrial electron transport by antimycin A treatment (24 h) also decreased the I_{Kir}. The ρ0 myoblasts showed depolarized resting membrane potential and higher basal [Ca²⁺]_i. Our results demonstrated the specific downregulation of I_{Kir} by dysfunctional mitochondria. The resultant depolarization and altered Ca²⁺ signaling might be associated with impaired myoblast fusion in ρ0 myoblasts.

INTRODUCTION

Mononucleated myoblasts are differentiated into multinucleated myofibers through processes including cell fusion. The myoblast differentiation (myogenesis) is a critical process of skeletal muscle formation and regeneration after muscle damage [1,2]. During myogenesis, intracellular Ca²⁺ signaling is known to be critical for the fusion of myoblasts [3]. Appropriate and timely increase of intracellular Ca²⁺ concentration ([Ca²⁺]_i) activates several myogenic transcription factors, including myogenin, myocyte enhancer factor-2 (MEF2), and nuclear factor of activated T-cells cytoplasmic 3 (NFATc3) [4-6].

Ca²⁺ channels are vital for maintaining elevated [Ca²⁺]_i. In myoblasts, both Ca²⁺ release-activated Ca²⁺ (CRAC) channels and voltage-operated Ca²⁺ channels (VOCCs) contribute to the Ca²⁺ signal [7-9]. Among the types of VOCCs, the T-type Ca²⁺ channel is considered important for myoblast fusion [8,9]. While VOCCs are activated by membrane depolarization, CRAC channels are voltage-independent channels and require membrane hyperpolarization to maintain the electromotive force for Ca²⁺ influx. Therefore, the functional levels of K⁺ channels would differentially affect [Ca²⁺]_i depending on the context of myogenesis signals; the depolarized resting membrane potential (RMP) would allow more Ca²⁺ influx as the membrane potential enters the window



This is an Open Access article distributed under the terms of the Creative Commons Attribution Non-Commercial License, which permits unrestricted non-commercial use, distribution, and reproduction in any medium, provided the original work is properly cited. Copyright © Korean J Physiol Pharmacol, pISSN 1226-4512, eISSN 2093-3827

Author contributions: S.J.K., W.L., and J.H.N. conceived and supervised the study; J.H.W., H.J.K., E.J.L., and I.C. designed the experiments; J.H.W., H.J.K., and E.J.L. performed the experiments; J.H.W., H.J.K., E.J.L., I.C., S.J.K., Y.K.K., W.L., and J.H.N. analyzed and interpreted the data; and S.J.K., W.L. and J.H.N. wrote the manuscript.

range of T-type Ca^{2+} channels. Myoblasts have been reported to express intermediate-conductance Ca^{2+} -activated K^+ channels (I_{KCa}) and inwardly-rectifying K^+ channels (Kir) [8,10-12].

The mitochondria generally produce most of the ATP in cells, and contribute to the regulation of intracellular Ca^{2+} signaling [13]. Previous studies demonstrated that mitochondrial DNA (mtDNA)-depleted ($\rho 0$) myoblasts or myoblasts treated with mitochondrial metabolic inhibitors show higher $[\text{Ca}^{2+}]_i$ levels than untreated myoblasts, even in the basal state [14,15]. This phenomenon could be due to multiple factors such as reduced Ca^{2+} storing capability of endoplasmic reticulum (ER), decreased mitochondrial Ca^{2+} uptake, and attenuated Ca^{2+} removal via the plasma membrane [15]. Apart from the lack of energy because of mitochondrial depletion, changes in the abovementioned ion channel functions might also lead to the abnormal Ca^{2+} influx in the $\rho 0$ myoblasts. However, no previous study has directly investigated the electrophysiological changes in $\rho 0$ myoblasts

In this study, we examined the effect of prolonged mitochondrial dysfunction on the ionic currents through VOCC (I_{VOCC}), Ca^{2+} -activated I_{KCa} , and Kir (I_{Kir}) using the whole-cell patch clamp technique in control and $\rho 0$ myoblasts. Our results demonstrate, first the first time, selective suppression of Kir and depolarized RMP in the $\rho 0$ myoblasts that fail to differentiate into myofibers.

METHODS

Myoblast culture and mtDNA depletion

L6 rat skeletal myocytes stably expressing GLUT4 (L6 myoblasts) were obtained from Karafast (Boston, MA, USA). The mtDNA-depleted L6 myoblasts were culture and generation using a method described in a previous report [16]. Briefly, for the quantification of mtDNA content, real-time PCR was routinely conducted to monitor the amounts of cytochrome oxidase I (COXI), COXII, and COXIV in DNA using a method described previously [16]. For myoblast differentiation, L6 myoblasts were transferred to differentiation medium containing 2% horse serum, 100 U/ml penicillin, and 100 $\mu\text{g}/\text{ml}$ streptomycin (all from

Life Technologies, Carlsbad, CA, USA) in MEM- α .

RNA extraction and real-time PCR

RNA extraction and cDNA synthesis were carried out as previously described [16]. Briefly, RNA was extracted from EtBr/uridine-treated or non-treated cells using Trizol reagent (Thermo Fisher Scientific, Waltham, MA, USA). Then, 1 μg of RNA was primed with oligo (dT) 20 primer (Bioneer, Daejeon, Republic of Korea) and reverse-transcribed at 42°C for 50 min and 72°C for 15 min. Gene-specific primers and 2 μl cDNA were used for the PCR analysis using a 7500 real-time PCR system, with Power SYBR[®] Green PCR Master Mix (both from Applied Biosystems, Foster City, CA, USA). The primer sequence details are provided in Table 1.

Western blotting

Protein was isolated using RIPA buffer supplemented with protease inhibitor (both from Thermo Fisher Scientific). Then 40 μg protein was electrophoresed on an 8% polyacrylamide gel containing SDS and transferred onto a nitrocellulose membrane (Millipore, Billerica MA, USA), which was then blocked with 5% BSA in Tris-buffered saline plus Tween (TBST) for 1 h. The membrane was incubated with anti-KIR2.1 (1:600) and anti- β -actin (1:2000; both from Santa Cruz Biotechnology, Santa Cruz, CA, USA) antibodies in 1% BSA or skim milk overnight. After washing with TBST, the blots were incubated with HRP-conjugated secondary antibody (Santa Cruz Biotechnology) for 1 h at room temperature (22-25°C) and developed using Super Signal West Pico Chemiluminescent Substrate (Thermo Fisher Scientific).

Electrophysiology

Cells were transferred into a bath mounted on the stage of an inverted microscope (TE2000-S, Nikon, Tokyo, Japan). The bath (-0.15 ml) was superfused at 3 ml/min, and voltage-clamp experiments were performed at room temperature (22-25°C). Patch pipettes with a free-tip resistance of approximately 3.5 and 4 M Ω

Table 1. DNA sequence of primers and optimal RT-PCR conditions

Gene identity	Primers	Annealing Temp (°C)	Optimal No. of cycles ^a
β -actin	Forward: 5'-ttgtaaccaactgggacgatatgg-3' Reverse: 5'-gatcttgatctcatgggtgtagg-3'	60	25
Cytochrome c oxidase 1 (COX1)	Forward: 5'-gcctagatgtagacacccgagcc-3' Reverse: 5'-cgacaggatccctgctaacc-3'	60	25
Cytochrome c oxidase 2 (COX2)	Forward: 5'-caagacgctacacacctatc-3' Reverse: 5'-ctaatagacgaagtccacctgg-3'	60	25
Cytochrome c oxidase 4 (COX4)	Forward: 5'-gcagtggcagaatgttgctacc-3' Reverse: 5'-cacagcagcaggctctcacttc-3'	60	25

^aFor quantitative real-time RT-PCR, the number of cycles was increased up to 37.

were used for whole-cell patch-clamp assays. To measure ionic currents, conventional whole-cell patch-clamp recordings were conducted using an Axopatch 200B amplifier (Molecular Devices, Sunnyvale, CA, USA). To determine the membrane potential, current-clamp experiments were carried out using a nystatin-perforated whole-cell configuration. For nystatin treatment, the nystatin stock was sonicated and diluted in a pipette solution to a final concentration of 60-70 $\mu\text{g/ml}$. Nystatin was freshly prepared on each day of the experiments. The recorded data were digitalized at 5 kHz and low-pass-filtered using a Digidata 1440A (Molecular Devices). Patch pipettes were fabricated from borosilicate glass (World Precision Instruments, Sarasota, FL, USA) using a five step programmable Flaming-Brown puller (Model P-97, Shutter Instruments, Novato, CA, USA). A pulled pipette was fabricated to facilitate giga-seal formation using a microforge (Narishige, Tokyo, Japan). pCLAMP software v9.2 and Digidata-1322A (Molecular Devices) were used to acquire data and apply command pulses. Voltage and current trace data were saved on a desktop computer and analyzed using Clampfit Software 10.4 (Molecular Devices), Prism 6.0 (GraphPad Software, La Jolla, CA, USA), and Origin 8.0 (MicroCal, Northampton, MA, USA).

$[\text{Ca}^{2+}]_i$ measurements

$[\text{Ca}^{2+}]_i$ was measured in HEPES-buffered physiological salt solution (PSS) containing 145 mM NaCl, 3.6 mM KCl, 10 mM HEPES, 1.3 mM CaCl_2 , 1 mM MgCl_2 , and 5 mM D-glucose (pH 7.4). Cells were harvested in a normal bath solution, loaded with fura-2 acetoxymethyl ester (fura-2, 5 μM , 30 min, 25°C), and washed once with fresh PSS. Fluorescence was monitored in a stirred quartz microcuvette (1 ml) in the temperature-controlled

cell holder of a fluorescence spectrophotometer (Photon Technology Instrument, Birmingham, NJ, USA) at wavelengths of 340 and 380 nm (excitation) and 510 nm (emission). The calibration of Ca^{2+} concentrations was described in a previous report [17].

Solutions

Normal Tyrode's bath solution for the whole-cell patch-clamp assay contained 145 mM NaCl, 3.6 mM KCl, 1 mM MgCl_2 , 1.3 mM CaCl_2 , 10 mM glucose, and 10 mM HEPES, at a pH of 7.4 (adjusted with NaOH). The high- K^+ solution for whole-cell patch clamp contained 145 mM KCl, 1 mM MgCl_2 , 1 mM CaCl_2 , 10 mM glucose, and 10 mM HEPES, at a pH of 7.4 (adjusted with NaOH). The pipette solution for whole-cell patch clamp contained 145 mM KCl, 3 mM MgCl_2 , 10 mM HEPES, 3 mM ATP magnesium salt, and 1 mM EGTA, at a pH of 7.2 (adjusted with KOH). The pipette solution of 1 μM free Ca^{2+} contained 135 mM KCl, 8.7 mM CaCl_2 , 1 mM MgCl_2 , 10 mM EGTA, 5 mM HEPES, and 3 mM ATP, at a pH of 7.2 (adjusted with KOH).

Statistical analysis

All results were analyzed using the GraphPad Prism 6.0 and Origin 8.0 software programs, and the data are expressed as the mean \pm standard error of the mean. Means of the control and $\rho 0$ myoblast groups were compared using an unpaired t-test and a $p < 0.05$ was considered statistically significant.

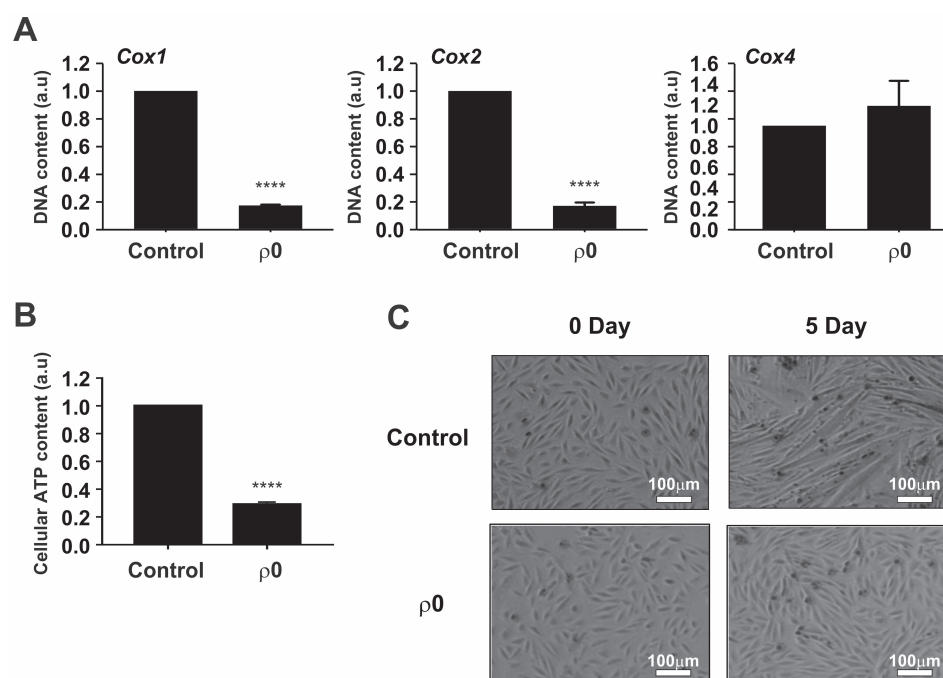


Fig. 1. Characterization of mtDNA-depleted L6 GLUT4myc myocytes. (A) Comparison of cytochrome oxidase I (COX1), COX2, and COX4 levels between normal L6 GLUT4myc myocytes (control) and mtDNA-depleted L6 GLUT4myc myocytes ($\rho 0$ myoblasts) using real-time PCR. Relative intensities are presented as normalized values with the intensity of control set to 1. **** $p < 0.0001$. (B) Comparison of total cellular ATP level between control and $\rho 0$ myoblasts. ATP contents expressed as normalized value, which was set to 1. **** $p < 0.0001$. (C) Comparison of differentiation of myoblasts into myotubes between control and $\rho 0$ myoblasts.

RESULTS

To confirm the mitochondrial reduction, we determined the relative amounts of mtDNA (COX1 and COX2) and nuclear DNA (COX4). The levels of COX1 and COX2 in $\rho 0$ myoblasts were $\leq 20\%$ of those in the control myoblasts, whereas the level of COX4 was unchanged (Fig. 1A). In addition, the total cellular ATP content of the $\rho 0$ myoblasts was approximately 30% of that of the control myoblasts, indicating impaired mitochondrial function (Fig. 1B). Five days of culture in horse serum-free medium induced differentiation of control myoblasts, but not $\rho 0$ cells, into myotubes (Fig. 1C).

Ionic currents in $\rho 0$ myoblasts

To record the VOCC current, whole-cell patch clamp was conducted using a CsCl-rich pipette solution. Depolarizing step pulses from a holding voltage of -80 mV revealed transient inward currents from above -50 mV (Fig. 2A, inset). Plotting the peak amplitudes of I_{VOCC} density (pA/pF) according to the test voltages revealed typical U-shape I/V curve of VOCC (Fig. 2A). The current densities of VOCC were not different between $\rho 0$ and control cells; -35.5 ± 7.44 pA/pF and -25.5 ± 3.65 pA/pF at 0 mV in control and $\rho 0$ myoblasts, respectively (Fig. 2B).

To record I_{KCa} , KCl-rich pipette solution with increased Ca^{2+} activity ($1 \mu\text{M}$ free Ca^{2+} clamped with 10 mM EGTA) was adopted. Ramp-like depolarization from -100 to 100 mV revealed voltage-independent large outward currents, consistent with the known property of I_{KCa} (Fig. 2C). The amplitudes of I_{KCa} density were

quite variable, but not statistically different between control and $\rho 0$ myoblasts; 208.8 ± 34.92 pA/pF and 265.8 ± 44.39 pA/pF at $+25$ mV, respectively (Fig. 2D).

To record the I_{Kir} , Ca^{2+} -free KCl pipette solution and 145 mM KCl bath solution were used for the whole-cell patch clamp applying ramp-like pulse from -140 to 70 mV. Under similar KCl conditions, large inward K^+ currents were recorded at the negative clamp voltage range, and the I/V curves showed typical inward rectification property (Fig. 3A). Interestingly, I_{Kir} was largely decreased in $\rho 0$ myoblasts (Figs. 3A and B). The current densities were -50.6 ± 15.81 pA/pF and -13.6 ± 5.42 pA/pF at -120 mV in the control and $\rho 0$ myoblasts, respectively. For the molecular identity of Kir, the KIR2.1 channel is known to be expressed in myoblasts [10] and the immunoblot analysis revealed that its expression level was decreased by $31 \pm 0.1\%$ in the $\rho 0$ cells.

To elucidate the mechanism underlying the I_{Kir} decrease in $\rho 0$ myoblasts, normal myoblasts were treated with antimycin A ($10 \mu\text{M}$), a mitochondrial complex III inhibitor, for 24 h [18]. The density of I_{Kir} was also drastically decreased in the antimycin A-treated cells compared with that in untreated cells (Figs. 3D and E, -63.9 ± 13.35 pA/pF vs. -2.6 ± 2.08 pA/pF at -120 mV).

Depolarized RMP with higher resting $[\text{Ca}^{2+}]_i$ and decreased store-operated Ca^{2+} entry (SOCE) in $\rho 0$ myoblasts

To measure the RMP of myoblasts under physiological conditions, we used a nystatin-perforated patch clamp that preserved cellular components other than intracellular monovalent cations

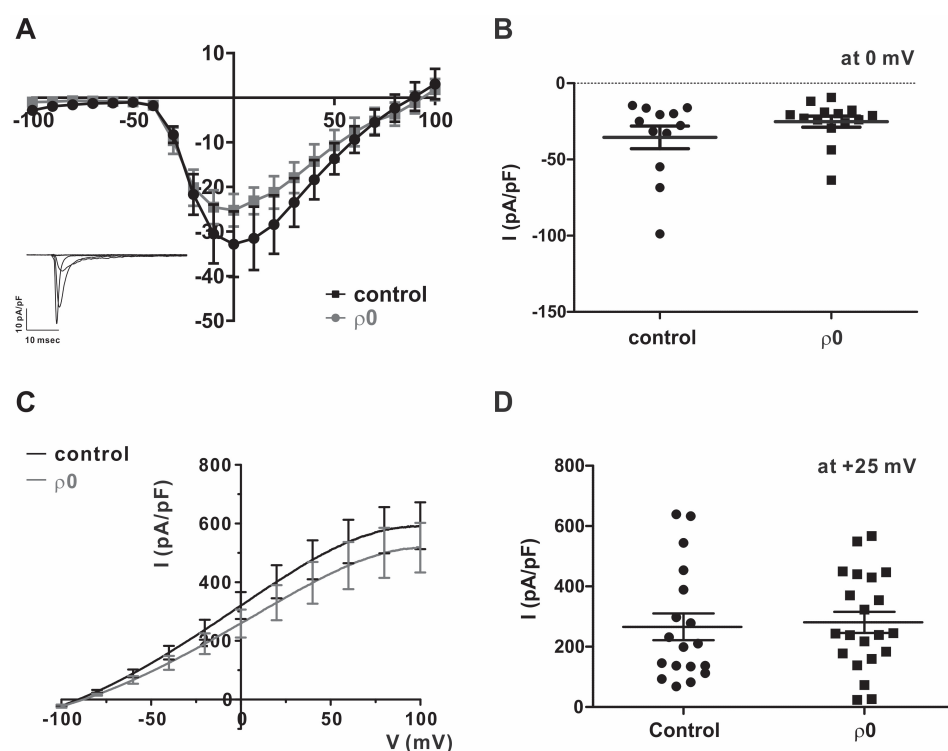


Fig. 2. Voltage-operated Ca^{2+} channel (VOCC) and Ca^{2+} activated K^+ channel are not affected by mtDNA depletion.

(A) Representative current traces of myocyte responses to each test pulse (inset). For whole-cell patch-clamp recordings, a test pulse was applied to myocytes for 500 ms, and voltage pulses were applied from the holding potential (-80 mV) in decrements or increments of $\Delta 10$ mV between -100 mV and 100 mV. Average current (I)-voltage (V) relationship curve for the peak VOCC current at each voltage in response to each test pulse between control ($n=12$) and $\rho 0$ myoblasts ($n=14$). (B) Summary of the current density of VOCC averaged at 0 mV. All data are means \pm standard error of the mean. (C) Average I-V relationship curve in control and $\rho 0$ myoblasts in response to $1 \mu\text{M}$ $[\text{Ca}^{2+}]_i$ pipette solution. (D) Summary of Ca^{2+} -activated K^+ current (I_{KCa}) at $+25$ mV in control and $\rho 0$ myoblasts.

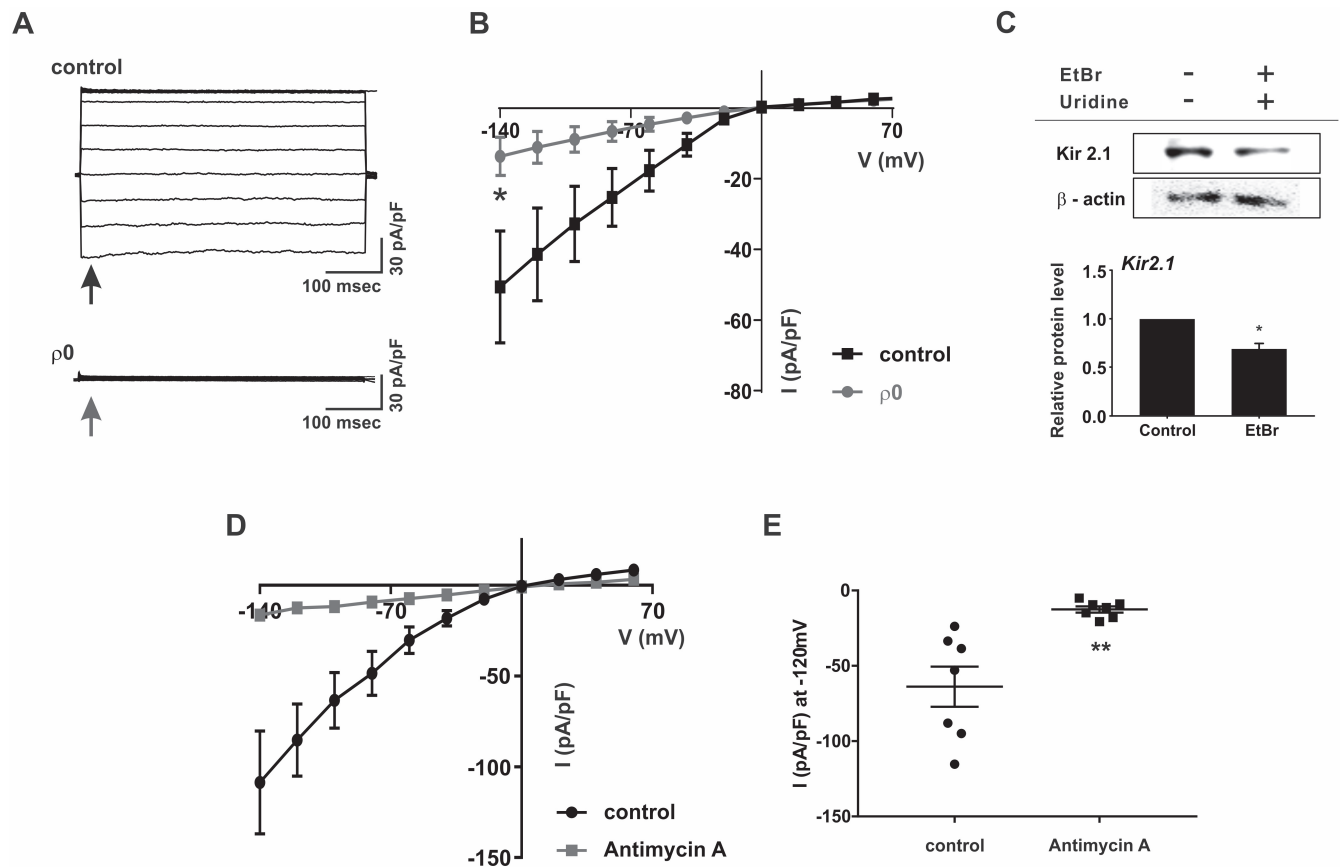


Fig. 3. Downregulation of inward-rectifying K^+ channel in $\rho 0$ myoblasts. (A) Representative chart trace recordings of inward-rectifying K^+ current (I_{kir}) in symmetrical KCl solution. For whole-cell patch-clamp recordings, the current was obtained by step depolarizing pulse ranging from -140 mV to 70 mV at a holding potential of 0 mV. (B) Average I-V relationship curve for the peak I_{kir} from -140 to 70 mV between control ($n=13$) and $\rho 0$ myoblasts ($n=13$). $*p<0.05$. (C) Immunoblot assay of KIR2.1 and β -actin expression in control and $\rho 0$ myoblasts. KIR2.1 signals were normalized to the β -actin signal, and mean values are displayed as bar graphs ($n=3$). $*p<0.05$. Data are means \pm standard error of the mean. (D) Average I-V relationship curve of I_{kir} following treatment with antimycin A ($n=7$) and in control myoblasts ($n=7$) in normal myocytes. (E) Current density of I_{kir} at -120 mV. $**p<0.01$. All data are presented as the mean \pm standard error of the mean.

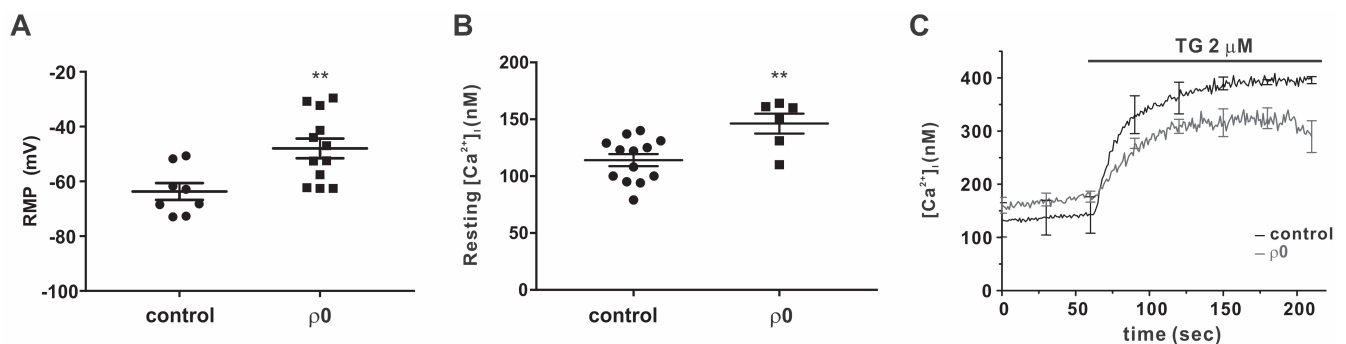


Fig. 4. Resting membrane potential (RMP) is depolarized and store-operated Ca^{2+} entry (SOCE) is diminished in $\rho 0$ myoblasts. (A) Comparison of RMP between control ($n=8$) and $\rho 0$ myoblasts ($n=12$). (B) Average $[Ca^{2+}]_i$ between control ($n=13$) and $\rho 0$ myoblasts ($n=6$) in the resting state. (C) Average trace recordings of $[Ca^{2+}]_i$, which increased following thapsigargin ($2 \mu M$) treatment of control (black) and $\rho 0$ (gray) myoblasts. Data are means \pm standard error of the mean ($n=3$). $**p<0.01$.

[19]. Consistent with the decrease in I_{kir} , the RMP of $\rho 0$ myoblasts was more depolarized than that of the control; -63.7 ± 3.06 mV vs. -47.9 ± 3.6 mV (Fig. 4A). Moreover, in accordance with a previous study [15], the resting $[Ca^{2+}]_i$ in $\rho 0$ myoblasts was higher than that

in control myoblasts was (146.2 ± 8.74 nM vs. 114.1 ± 5.31 nM, Fig. 4B).

We also assessed SOCE from the sustained increased in $[Ca^{2+}]_i$ induced by thapsigargin (TG, $2 \mu M$), which inhibits the sarco/endoplasmic

mic reticulum Ca^{2+} -ATPase inhibitor. The TG-induced $[\text{Ca}^{2+}]_i$ increase ($\Delta[\text{Ca}^{2+}]_i$), a parameter reflecting steady-stated store-operated Ca^{2+} entry (SOCE), was slightly lower in $\rho 0$ than it was in control myoblasts (Fig. 4C, $\Delta[\text{Ca}^{2+}]_i$ at 200 sec was 260.6 ± 24.83 nM and 152 ± 26.23 nM in the control and $\rho 0$ myoblasts, respectively, $p < 0.05$).

DISCUSSION

In this study, we found, for the first time, markedly decreased I_{Kir} along with altered $[\text{Ca}^{2+}]_i$ and SOCE in mtDNA-depleted myoblasts. Since the $\rho 0$ myoblasts did not differentiate into myotubes, the results suggest that Kir might be a myogenesis-related ion-channel that regulates intracellular Ca^{2+} signaling, although indirectly.

Since Ca^{2+} influx through the VOCC is known to be critical for the fusion of myoblasts [9], we initially anticipated a decrease in I_{VOCC} in the $\rho 0$ myoblasts, however, this was not the case. In excitable cells, the activation of I_{KCa} facilitates repolarization when the $[\text{Ca}^{2+}]_i$ is above the threshold level. In the $\rho 0$ myoblasts, I_{KCa} density at the fixed concentration was not altered. Although more experiments are warranted, the results further emphasize the effects of the dramatic decrease in I_{Kir} . It has been reported that the ether-a-go-go-related gene (ERG) channel, a member of the voltage-gated K^+ channel family is expressed in myoblasts [8,20]. However, we did not observe significant levels of the putative ERG channel current in L6 myoblasts (data not shown).

Because I_{Kir} is important in setting the RMP in many types of excitable cells, the dramatic decrease in I_{Kir} and the downregulation of KIR2.1 in $\rho 0$ myoblasts were interesting findings. However, compared to the functional decrease of I_{Kir} , the immunoblot assays showed that the decrease in KIR2.1 expression of the total cell lysate was relatively less significant (Fig. 3). More specific assays of KIR2.1 in the plasma membrane might facilitate a more precise correlation between the I_{Kir} protein expression and function.

Interestingly, pharmacological inhibition of the mitochondrial electron transport chain (ETC) complex III by antimycin A also induced similar decrease in the I_{Kir} . Although it is unclear how functional inhibition of the mitochondria selectively decreased the I_{Kir} in myoblasts, the effects of antimycin A treatment also suggested that sustained inhibition of oxidative phosphorylation, i.e., ATP depletion, appeared critical for maintaining KIR2.1 expression. The KIR2.1 activity is well known to be sensitively regulated by membrane phosphatidylinositol(4,5)-bisphosphate (PIP_2) [21,22]. Since the production of PIP_2 by PI kinase requires ATP, the reduced intracellular ATP induced by mtDNA depletion or antimycin treatment might have decreased PIP_2 in the cell membranes, thereby reducing the activity and functions of KIR2.1.

Recently, it was reported that activation of AMPK, a critical

intracellular metabolic sensor with various signaling functions, may be implicated in the downregulation of KIR2.1. Particularly, the activation of AMPK by ATP-depletion or increase in the cytosolic Ca^{2+} activity decreases KIR2.1 abundance in the cell membrane of *Xenopus* oocytes through the activation of the AMPK by activating the ubiquitin ligase Nedd4-2 [23]. Recently, Zhao et al. [24] reported that mitochondrial dysfunction induced by genetic defects or mitochondria-targeted antioxidants activates AMPK signaling in human keratinocytes. Therefore, activation of AMPK might be one of the mechanisms underlying the I_{Kir} decay in the present study [24]. In agreement with previous results [24], we also observed increased expression and phosphorylation of AMPK in the mtDNA-depleted myocytes in this study (data not shown). Therefore, further studies would be essential to elucidate the exact mechanisms underlying the inhibition of KIR2.1 activity by prolonged mitochondrial inhibition.

Although proper Ca^{2+} signaling is known to be required for the differentiation of myoblasts, the abnormal or untimely increase in basal $[\text{Ca}^{2+}]_i$ might have hampered the differentiation of the $\rho 0$ myoblasts in the present study. Considering the robust activity of VOCC, the higher resting $[\text{Ca}^{2+}]_i$ might, at least partly, be due to the I_{Kir} decrease and membrane depolarization, as partial depolarization of the RMP would increase the Ca^{2+} influx via VOCCs [25,26]. Another plausible mechanism underlying the resting $[\text{Ca}^{2+}]_i$ increase could be impaired ATP supply to the various active Ca^{2+} transporters such as SERCA, which should also be considered for proper interpretation of the findings.

It has also been suggested that the so-called Ca^{2+} release-activated Ca^{2+} (CRAC) channel is important for myogenesis [7]. Since CRAC channels are mainly responsible for the Ca^{2+} influx pathway of SOCE, the lower SOCE in $\rho 0$ myoblasts also attracted our attention. However, since we did not directly measure the electrical Ca^{2+} current through CRAC channels in L6 myoblasts, the implication of partial decrease in the thapsigargin-induced $\Delta[\text{Ca}^{2+}]_i$ could not be provided here. Since the maximum levels of $[\text{Ca}^{2+}]_i$ were not significantly different between the control and $\rho 0$ myoblasts (392.28 ± 2.45 nM and 328.13 ± 21.94 , respectively, $p > 0.05$, Fig. 4C), we cautiously suggest that the decrease in I_{Kir} and partial depolarization might be partly responsible for the lower SOCE in $\rho 0$ myoblasts induced by reducing the electromotive driving force of the Ca^{2+} influx. Furthermore, the higher basal $[\text{Ca}^{2+}]_i$ would have inactivated the CRAC channels [27]. To avoid the complexity of Ca^{2+} -induced inactivation of CRAC channels, we measured the SOCE using the Ca^{2+} -add back protocol (i.e., thapsigargin was applied after incubating the cells under Ca^{2+} -free conditions, and then Ca^{2+} was added to the bath), which would more precisely reflect the maximum SOCE. The exact implication of the higher basal $[\text{Ca}^{2+}]_i$ with lower SOCE in $\rho 0$ myoblasts would also require further studies using patch clamp and a more rigorous protocol for SOCE measurement.

ACKNOWLEDGEMENTS

This work was supported by a National Research Foundation of Korea (NRF) grant funded by the Ministry of Science, ICT and Future Planning (MIST) of the Korean government (grant number NRF-2015R1C1A1A02037738).

CONFLICTS OF INTEREST

The authors declare no conflicts of interest.

REFERENCES

- Abmayr SM, Pavlath GK. Myoblast fusion: lessons from flies and mice. *Development*. 2012;139:641-656.
- Buckingham M. Skeletal muscle formation in vertebrates. *Curr Opin Genet Dev*. 2001;11:440-448.
- David JD, See WM, Higginbotham CA. Fusion of chick embryo skeletal myoblasts: role of calcium influx preceding membrane union. *Dev Biol*. 1981;82:297-307.
- Black BL, Olson EN. Transcriptional control of muscle development by myocyte enhancer factor-2 (MEF2) proteins. *Annu Rev Cell Dev Biol*. 1998;14:167-196.
- Friday BB, Pavlath GK. A calcineurin- and NFAT-dependent pathway regulates Myf5 gene expression in skeletal muscle reserve cells. *J Cell Sci*. 2001;114:303-310.
- Molkentin JD, Olson EN. Combinatorial control of muscle development by basic helix-loop-helix and MADS-box transcription factors. *Proc Natl Acad Sci U S A*. 1996;93:9366-9373.
- Darbellay B, Arnaudeau S, König S, Jousset H, Bader C, Demaurex N, Bernheim L. STIM1- and Orail1-dependent store-operated calcium entry regulates human myoblast differentiation. *J Biol Chem*. 2009;284:5370-5380.
- Cooper E. A new role for ion channels in myoblast fusion. *J Cell Biol*. 2001;153:F9-12.
- Bijlenga P, Liu JH, Espinos E, Haenggeli CA, Fischer-Lougheed J, Bader CR, Bernheim L. T-type $\alpha 1H$ Ca^{2+} channels are involved in Ca^{2+} signaling during terminal differentiation (fusion) of human myoblasts. *Proc Natl Acad Sci U S A*. 2000;97:7627-7632.
- Fischer-Lougheed J, Liu JH, Espinos E, Mordasini D, Bader CR, Belin D, Bernheim L. Human myoblast fusion requires expression of functional inward rectifier Kir2.1 channels. *J Cell Biol*. 2001;153:677-686.
- Konig S, Béguet A, Bader CR, Bernheim L. The calcineurin pathway links hyperpolarization (Kir2.1)-induced Ca^{2+} signals to human myoblast differentiation and fusion. *Development*. 2006;133:3107-3114.
- Tanaka S, Ono Y, Sakamoto K. DCEBIO facilitates myogenic differentiation via intermediate conductance Ca^{2+} activated K^{+} channel activation in C2C12 myoblasts. *J Pharmacol Sci*. 2017;133:276-279.
- Friedman JR, Nunnari J. Mitochondrial form and function. *Nature*. 2014;505:335-343.
- Wagatsuma A, Sakuma K. Mitochondria as a potential regulator of myogenesis. *Sci World J*. 2013;2013:593267.
- Biswas G, Adebajo OA, Freedman BD, Anandatheerthavarada HK, Vijayarathy C, Zaidi M, Kotlikoff M, Avadhani NG. Retrograde Ca^{2+} signaling in C2C12 skeletal myocytes in response to mitochondrial genetic and metabolic stress: a novel mode of inter-organelle crosstalk. *EMBO J*. 1999;18:522-533.
- Park SY, Choi GH, Choi HI, Ryu J, Jung CY, Lee W. Depletion of mitochondrial DNA causes impaired glucose utilization and insulin resistance in L6 GLUT4myc myocytes. *J Biol Chem*. 2005;280:9855-9864.
- Nam JH, Lee DU. Foeniculum vulgare extract and its constituent, trans-anethole, inhibit UV-induced melanogenesis via ORAI1 channel inhibition. *J Dermatol Sci*. 2016;84:305-313.
- Ma X, Jin M, Cai Y, Xia H, Long K, Liu J, Yu Q, Yuan J. Mitochondrial electron transport chain complex III is required for antimycin A to inhibit autophagy. *Chem Biol*. 2011;18:1474-1481.
- Okada Y. Patch clamp techniques: from beginning to advanced protocols. Tokyo: Springer; 2012.
- Bernheim L, Bader CR. Human myoblast differentiation: Ca^{2+} channels are activated by K^{+} channels. *News Physiol Sci*. 2002;17:22-26.
- D'Avanzo N, Cheng WW, Doyle DA, Nichols CG. Direct and specific activation of human inward rectifier K^{+} channels by membrane phosphatidylinositol 4,5-bisphosphate. *J Biol Chem*. 2010;285:37129-37132.
- Kim KS, Jang JH, Lin H, Choi SW, Kim HR, Shin DH, Nam JH, Zhang YH, Kim SJ. Rise and fall of Kir2.2 current by TLR4 signaling in human monocytes: PKC-dependent trafficking and PI3K-mediated PIP_2 decrease. *J Immunol*. 2015;195:3345-3354.
- Alesutan I, Munoz C, Sopjani M, Dërmaku-Sopjani M, Michael D, Fraser S, Kemp BE, Seeböhm G, Föllner M, Lang F. Inhibition of Kir2.1 (KCNJ2) by the AMP-activated protein kinase. *Biochem Biophys Res Commun*. 2011;408:505-510.
- Zhao B, Qiang L, Joseph J, Kalyanaraman B, Viollet B, He YY. Mitochondrial dysfunction activates the AMPK signaling and autophagy to promote cell survival. *Genes Dis*. 2016;3:82-87.
- Engbers JD, Anderson D, Zamponi GW, Turner RW. Signal processing by T-type calcium channel interactions in the cerebellum. *Front Cell Neurosci*. 2013;7:230.
- Lee N, Jeong S, Kim KC, Kim JA, Park JY, Kang HW, Perez-Reyes E, Lee JH. Ca^{2+} regulation of Cav3.3 T-type Ca^{2+} channel is mediated by calmodulin. *Mol Pharmacol*. 2017;92:347-357.
- Scrimgeour NR, Wilson DP, Barritt GJ, Rychkov GY. Structural and stoichiometric determinants of Ca^{2+} release-activated Ca^{2+} (CRAC) channel Ca^{2+} -dependent inactivation. *Biochim Biophys Acta*. 2014;1838:1281-1287.